

Article

# Nanoporous Carbon Materials Derived from Washnut Seed with Enhanced Supercapacitance

Ram Lal Shrestha <sup>1</sup>, Timila Shrestha <sup>1</sup>, Birendra Man Tamrakar <sup>2</sup>, Rekha Goswami Shrestha <sup>3,\*</sup> , Subrata Maji <sup>3</sup>, Katsuhiko Ariga <sup>3,4</sup>  and Lok Kumar Shrestha <sup>3,\*</sup> 

<sup>1</sup> Department of Chemistry, Amrit Campus, Tribhuvan University, Kathmandu 44613, Nepal; swagatstha@gmail.com (R.L.S.); timilastha@gmail.com (T.S.)

<sup>2</sup> Department of Chemistry, Tri-Chandra Multiple Campus, Tribhuvan University, Kathmandu 44600, Nepal; tamrakar\_birendra@hotmail.com

<sup>3</sup> International Center for Materials Nanoarchitectonics (WPI-MANA), National Institute for Materials Science (NIMS), 1-1 Namiki, Ibaraki 305-0044, Japan; MAJI.Subrata@nims.go.jp (S.M.); ARIGA.Katsuhiko@nims.go.jp (K.A.)

<sup>4</sup> Graduate School of Frontier Sciences, The University of Tokyo, 5-1-5 Kashiwanoha, Kashiwa, Chiba 277-8561, Japan

\* Correspondence: rekhashrestha3@hotmail.com (R.G.S.); SHRESTHA.Lokkumar@nims.go.jp (L.K.S.); Tel.: +81-29-860-4809 (L.K.S.)

Received: 21 April 2020; Accepted: 19 May 2020; Published: 21 May 2020



**Abstract:** Nanoporous activated carbons-derived from agro-waste have been useful as suitable and scalable low-cost electrode materials in supercapacitors applications because of their better surface area and porosity compared to the commercial activated carbons. In this paper, the production of nanoporous carbons by zinc chloride activation of Washnut seed at different temperatures (400–1000 °C) and their electrochemical supercapacitance performances in aqueous electrolyte (1 M H<sub>2</sub>SO<sub>4</sub>) are reported. The prepared nanoporous carbon materials exhibit hierarchical micro- and meso-pore architectures. The surface area and porosity increase with the carbonization temperature and achieved the highest values at 800 °C. The surface area was found in the range of 922–1309 m<sup>2</sup> g<sup>-1</sup>. Similarly, pore volume was found in the range of 0.577–0.789 cm<sup>3</sup> g<sup>-1</sup>. The optimal sample obtained at 800 °C showed excellent electrochemical energy storage supercapacitance performance. Specific capacitance of the electrode was calculated 225.1 F g<sup>-1</sup> at a low current density of 1 A g<sup>-1</sup>. An observed 69.6% capacitance retention at 20 A g<sup>-1</sup> indicates a high-rate capability of the electrode materials. The cycling stability test up to 10,000 cycles revealed the outstanding stability of 98%. The fascinating surface textural properties with outstanding electrochemical performance reveal that Washnut seed would be a feasible agro-waste precursor to prepare nanoporous carbon materials as a low-cost and scalable supercapacitor electrode.

**Keywords:** Washnut seed; chemical activation; micro/mesoporous carbon; supercapacitor

## 1. Introduction

Supercapacitors or electrical double-layer capacitors (EDLC), the most convenient and state-of-the-art electrochemical energy storage systems, with outstanding power density (>400 kW kg<sup>-1</sup>), unusually long cycle stability (>10,000), rapid charging-discharging with enhanced rate capability and poor internal resistance, and environmentally friendly and low-cost, have been extensively used for high power electronic devices [1–10]. In EDLCs, electrolyte ions are adsorbed at the electrode surface by fast dynamic propagation and form double layers of electrical charges [11]. Supercapacitors offer greater power densities compared to the traditional batteries and fuel cells; therefore, they have been implemented in industrial power and energy management systems [12,13]. However, compared

to batteries, supercapacitors exhibit low energy density, and hence, they have explored less in the potential technological applications [14,15]. The energy density of supercapacitors is based on the specific capacitance ( $C_s$ ) and the real operating potential window ( $V$ ). The specific capacitance directly depends on the properties of the materials used for the electrode and potential window depends on the electrolyte used for the construction of the supercapacitor cells [16,17]. Since the operating potential window is fixed in aqueous electrolyte ( $\sim 1.2$  V), it is important to improve the structure and properties of the materials to be used as supercapacitor electrodes so that introducing the novel and smart electrode materials could exhibit high specific capacitances and also induces good combination with electrolyte [18,19]. It is important to have a good match between electrolyte ions and pore size of the electrode material, and wettability of electrode and electrolyte conductivity [20].

Recently, nanoporous activated carbons have received considerable interest as the leading supercapacitor electrode materials because of the low production cost, outstanding cycle stability, and excellent surface specific surface area and porosity [21–25]. Different porous carbon materials have been produced either from synthetic carbon sources or natural biomasses by direct carbonization or chemical activation methods as well as template method and explored as supercapacitor electrode materials [26–30]. Of several methods, natural biomass or agricultural wastes-derived nanoporous carbons by physical and chemical activation methods represent the feasible, scalable, and low-cost method. Biomass-derived nanoporous activated carbons exhibit very high surface area and offer large porosity because of their unique hierarchical micro- and meso-porous architectures, and also have good electrical conductivity and excellent electrochemical stability, which are highly desired in the emerging electrochemical energy storage supercapacitors applications [31–33].

All the natural biomasses or agricultural wastes are lignocellulose materials containing cellulose, hemicellulose and lignin, which upon pyrolysis at lower temperatures (200–300 °C) under the air or nitrogen gas atmosphere produces biochar with a low specific surface area and low porosity. Therefore, the biochar is not useful in supercapacitors. Nevertheless, the biochar can be activated and transformed into high surface area hierarchical nanoporous carbon materials with well-developed porosity desired in supercapacitors by the direct carbonization and physical or chemical activation methods [34,35]. The industrial-scale manufacture of nanoporous activated carbons is based on the physical activation of the biochar at higher temperatures (800–1100 °C) under the flow of steam/or carbon dioxide. This is a simple and cost-effective fabrication process. Physically activated carbons exhibit specific surface area in the range of 500–1000 m<sup>2</sup> g<sup>-1</sup>. The surface area of the biomass-derived physically activated carbons can further be enhanced, which can be enabled by the chemical activation method and the resulting carbon materials achieve a surface area far more than 1000 m<sup>2</sup> g<sup>-1</sup> [36]. The chemical activation method includes the impregnation of biomass or biochar with an activating agent and then the mixture is carbonized in the temperature ranges of 400–1000 °C in an inert atmosphere of nitrogen or argon gas [37]. Activating agents generally include dehydrating salts, such as zinc chloride (ZnCl<sub>2</sub>), sodium carbonate (Na<sub>2</sub>CO<sub>3</sub>), and also acid and alkali. Lignocellulose undergoes pyrolytic decomposition upon mixing with these activating agents and porosity enhancement can be achieved as a result of the depolymerization and dehydration of the biochar. Of several activating reagents, ZnCl<sub>2</sub> is a widely used chemical activating agent, which dehydrates and accelerates the decomposition of carbonaceous materials during the carbonization process and also restricts the formation of tar giving a high yield carbon. ZnCl<sub>2</sub> contributes to creating a porous structure acting as a template; intercalated ZnCl<sub>2</sub> upon washing creates the void space in the carbon matrix. Recently, using various agricultural wastes or biomass such as rice husks [38], corncob [39,40], pistachio shell [41], pitch [42], bamboo [43], Batata leaves and stalks [44], Peanut dregs [45], Lapsi seed (*Choerospondias axillaris*) [46], etc. high surface area nanoporous carbons with large porosity, interconnected mesopores and uniform pore size distribution essentially required in supercapacitor applications have been produced.

In this paper, the synthesis of nanoporous activated carbons from Washnut seed agro-waste by the ZnCl<sub>2</sub> activation method and their electrochemical supercapacitance performance are reported. Electrochemical measurements were carried out on three-electrode cells in 1 M H<sub>2</sub>SO<sub>4</sub>. Pre-carbonized

Washnut seed powder (char) was impregnated with the activating agent,  $\text{ZnCl}_2$  at 1:1 weight ratio, and carbonizations were carried out at different temperatures from 400 to 1000 °C.  $\text{ZnCl}_2$ -activated Washnut seed-derived nanoporous carbons display a hierarchical porous architecture containing both the micro- and meso-porous and offer a high specific surface area ( $1309 \text{ m}^2 \text{ g}^{-1}$ ) and pore volume ( $0.789 \text{ cm}^3 \text{ g}^{-1}$ ). An increase in carbonization temperature increases the surface area giving the best surface textural properties at 800 °C. The working electrode prepared with the optimal carbon sample showed excellent supercapacitance performance with the high specific capacitance calculated  $225.1 \text{ F g}^{-1}$  at  $1 \text{ A g}^{-1}$ . The electrode sustained 69.6% capacitance retention at a high current density of  $20 \text{ A g}^{-1}$  showing the high-rate capability of the electrode. Furthermore, an outstanding cycling stability of 98% was recorded after 10,000 charging–discharging cycles demonstrating that Washnut seed could be an appropriate alternative low-cost biomass for the production scalable carbon electrodes for high-performance supercapacitors.

## 2. Materials and Methods

### 2.1. Preparation of Nanoporous Activated Carbons

Agro-waste Washnut seed was washed with distilled water, dried at 80 °C for 6 h and ground into the powder form in a mechanical crusher. The Washnut seed powder was pre-carbonized at 300 °C in air for 3 h. Pre-carbonized Washnut seed powder was mixed with  $\text{ZnCl}_2$ , a chemical activating agent at 1:1 weight ratio and carbonizations were carried out at different temperatures (400–1000 °C) under the nitrogen flux ( $120 \text{ cc min}^{-1}$ ) in a tube furnace (KOYO, Tokyo, Japan). Temperature ramp and hold time was set to  $5 \text{ }^\circ\text{C min}^{-1}$  and 3 h, respectively. The obtained nanoporous carbon samples were treated with a dilute hydrochloric acid solution (0.5 M HCl) for removing the unreacted zinc chloride followed by distilled water washing (several times). The product was dried in vacuum at 80 °C for 6 h and further grounded into fine powders, and sieved through 250  $\mu\text{m}$  mesh size. The obtained samples were referred to as WNC\_400, WNC\_600, WNC\_800, and WNC\_1000 depending on the carbonization temperature. For comparison, Washnut seed powder was also directly carbonized at 800 °C without an activating agent and the product is referred to as WNP\_800.

### 2.2. Characterizations

Washnut seed-derived nanoporous carbon materials were subjected to advanced characterizations. Surface morphology and the pore structure were studied by scanning electron microscopy (SEM: S-4800, Hitachi Co., Ltd. Tokyo, Japan). The S-4800 was operated at an operating voltage of 10 kV and a field emission current of 10  $\mu\text{A}$ . SEM samples were platinum-coated ( $\sim 2 \text{ nm}$ ) on a Hitachi S-2030 ion-coater, to avoid sample charging effects. For the structural determination, powder X-ray diffraction (XRD) patterns were recorded on a Rigaku X-ray diffractometer, RINT, Tokyo, Japan, operating the X-ray diffractometer at 25 °C in the range 10 to 50° at 40 kV and 40 mA with  $\text{Cu-K}\alpha$  radiation. Graphitization and defects of the carbon samples were studied by Raman scattering (Jobin-Yvon T64000 Raman spectrometer, Edison, NJ, USA). Sample on glass substrate were excited with a green laser (514.5 nm) at 0.01 mW power and exposed for 30 s. Fourier-transformed infrared (FTIR) spectra were recorded by KBr pellet method on a Nicolet 4700 (Thermo Electron Corporation, Waltham, MA, USA) at 25 °C. For the determination of surface textural properties (surface areas, pore volumes, average pore sizes, and pore size distributions, nitrogen adsorption/desorption isotherms were measured using on Quantachrome Autosorb-iQ2, Boynton Beach, FL, USA: an automatic adsorption instrument. Carbon sample ( $\sim 20 \text{ mg}$ ) was degassed at 120 °C for 24 h before measurements and isotherms were recorded at liquid nitrogen temperature 77.35 K. From the sorption isotherms, Brunauer–Emmett–Teller (BET) surface area, and pore size distributions were determined by Barrett–Joyner–Halenda (BJH: for mesopore) method and density functional theory (DFT: for micropore).

### 2.3. Electrochemical Measurements

Cyclic voltammetry (CV) and galvanostatic charge-discharge (CD) measurements were carried out in a three-electrode system in an aqueous (1 M H<sub>2</sub>SO<sub>4</sub>) solution at 25 °C to study the electrochemical supercapacitance performances of the Washnut-derived nanoporous activated carbons. Modified glassy carbon electrode (GCE, ALS Co., Ltd, Tokyo, Japan) was used as the working electrode. For the working electrode preparation, the GCE was mirror polished with alumina (Al<sub>2</sub>O<sub>3</sub>) slurry, sonicated in acetone for 10 min and cleaned with distilled water. The prepared carbon material was dispersed in water-ethanol (4:1) mixture (1 mg mL<sup>-1</sup>) by sonicating the mixture for 45 min in a bath sonicator (BRANSON 3510, Hampton, NH, USA). The obtained suspension (3 μL) was dropcast onto the GCE and dried at 60 °C for 6 h to evaporate the solvents. Nafion solution (5 μL: 5% in ethanol) was then added on top of the carbon materials on the GCE surface as a binder and dried at 80 °C in vacuum for 12 h before the electrochemical measurements. The CV and CD measurements were carried out on a CHI 850D work station (CH Instruments, Inc. Austin, TX, USA) using a platinum wire was used as a counter and Ag/AgCl as the reference electrode.

From CD profiles, specific capacitance was calculated as:

$$C_s = \frac{I \cdot t}{m \cdot \Delta V} \quad (1)$$

where  $C_s$ ,  $I$ ,  $t$ ,  $m$ , and  $\Delta V$ , respectively, represent the specific capacitance (F g<sup>-1</sup>), discharge current (A), discharge time (s), mass of active electrode materials (g), and the operating potential window ( $V_{\text{final}} - V_{\text{initial}}$ ).

### 3. Results and Discussion

Surface morphology and pore architecture of the ZnCl<sub>2</sub> activated Washnut seed-derived nanoporous carbon materials were studied by scanning electron microscopy (SEM) imaging. Figure 1 depicts typical SEM images of the activated samples WNC\_400, WNC\_600, WNC\_800, and WNC\_1000 both at low- and high-magnification modes. For comparison, SEM images of a directly carbonized sample (WNP\_800) without ZnCl<sub>2</sub> is also included. The SEM images at low magnification (Figure 1a,c,e,g,i) reveal the Washnut seed-derived carbons have irregular morphology with micron-size particles containing visible microporous surface structure. In the high-magnification SEM images (Figure 1b,d,f,h,j), the chemically activated carbon surface display hierarchical micro- and meso-pore architectures. While in the directly carbonized WNP\_800 sample, a significantly smaller number of visible micro/mesopores is observed. A marco-sized interconnected channel like surface morphology can be visible in the high-magnification images of WNC\_400 (Figure 1d), and WNC\_600 (Figure 1f). On the other hand, a rather uniform mesoporous surface with interconnected pore structure can be seen in the high-magnification SEM images of WNC\_800 (Figure 1h), and WNC\_1000 (Figure 1j).

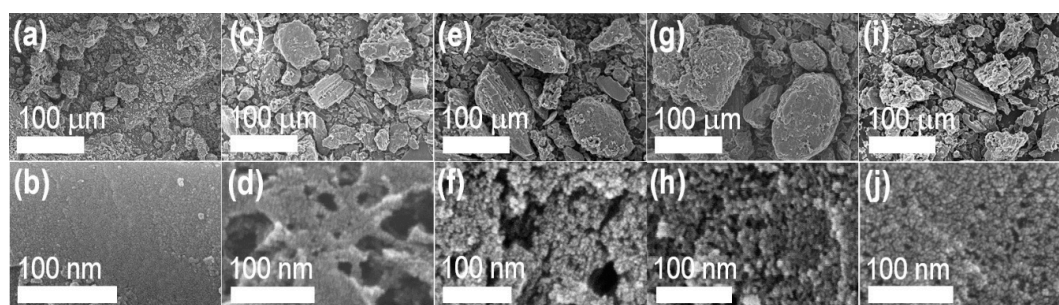


**Figure 1.** SEM images of Washnut seed-derived nanoporous activated carbons: (a,b) WNP\_800; (c,d) WNC\_400; (e,f) WNC\_600; (g,h) WNC\_800; (i,j) WNC\_1000.

Specific surface area, pore volumes, pore size distribution and average pore size were detected using nitrogen adsorption/desorption analysis. Figure 2a shows the nitrogen sorption isotherms of WNP\_800, WNC\_400, WNC\_600, WNC\_800, and WNC\_1000 measured at 77 K and Figure 2b,c show the pore size distributions estimated from the BJH and DFT method, respectively. The sorption isotherms reveal that all the chemically activated samples exhibit mixed Type-I/Type-IV isotherms, indicating the hierarchical micro- and meso-porous characteristics of the samples [47]. The strong nitrogen adsorption of chemically activated samples at lower relative pressure ( $P/P_0 < 0.03$ ) is the indication of plenty of micropores. While the hysteresis loops at higher relative pressures suggests that the samples also contain mesopore structure. Unlike the chemically activated samples, the sorption isotherm of the directly carbonized sample, WNP\_800, exhibits Type-III isotherm suggesting nonporous or microporous characteristics of the sample. The pore size distributions profiles (Figure 2b: obtained by BJH analysis; Figure 2c: obtained by DFT analysis) further confirm the presence of hierarchical micro- and meso-porous structures in the activated samples, WNC\_400, WNC\_600, WNC\_800, and WNC\_1000. The average micro- and meso-pore diameters are calculated 0.57 and 3.88 nm, respectively. These micro- and meso-pore distributions over the prepared carbon materials provide a sufficiently large surface area, where electrolyte ions can be adsorbed and also promotes the fast and easy diffusion in the electrode surface required in high energy storage systems [48].

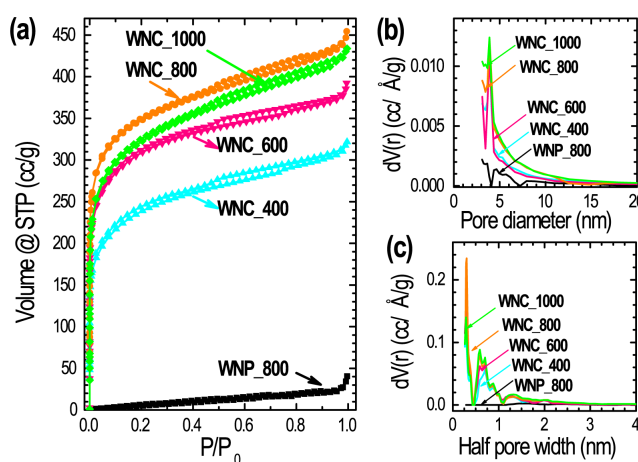


**Figure 2.** (a) Nitrogen sorption (adsorption/desorption) isotherms of WNP\_800, WNC\_400, WNC\_600, WNC\_800, and WNC\_1000 measured at 77 K, and the pore size distributions profiles obtained by (b) Barrett–Joyner–Halenda (BJH) method and (c) density functional theory (DFT) method.

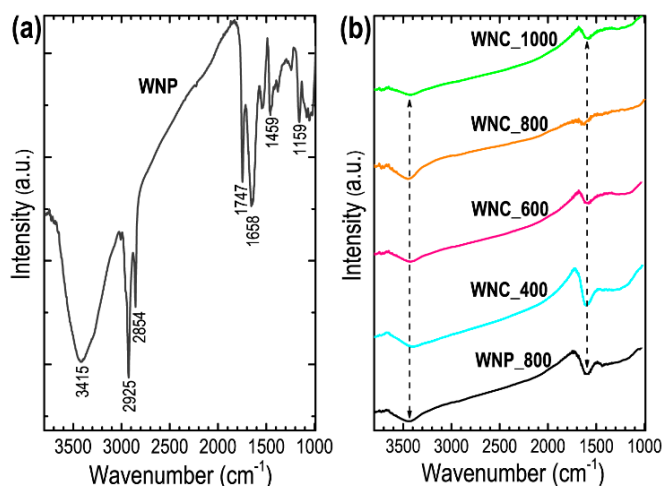
Due to the lack of well-developed porosity, specific surface area of the directly carbonized sample WNP\_800 is low ( $39.2 \text{ m}^2 \text{ g}^{-1}$ ). As a result, low energy storage performance is expected compared to the  $\text{ZnCl}_2$  activated samples. The surface textural properties of the prepared samples obtained from the nitrogen sorption analysis are presented in Table 1.

**Table 1.** Surface textural properties of the Washnut seed-derived nanoporous activated carbons.

Carbon Sample	SSA ( $\text{m}^2 \text{ g}^{-1}$ )	$S_{\text{micro}}$ ( $\text{m}^2 \text{ g}^{-1}$ )	$S_{\text{meso}}$ ( $\text{m}^2 \text{ g}^{-1}$ )	$V_p$ ( $\text{cm}^3 \text{ g}^{-1}$ )	$V_{\text{micro}}$ ( $\text{cm}^3 \text{ g}^{-1}$ )	$D_{\text{meso}}$ (nm)	$D_{\text{micro}}$ (nm)
WNP_800	39.2	15.3	23.9	0.099	0.037	3.09	–
WNC_400	922.4	836.5	85.9	0.577	0.444	3.88	0.573
WNC_600	1157.6	1080.5	77.1	0.662	0.535	3.88	0.548
WNC_800	1309.8	1196.1	113.7	0.798	0.618	3.88	0.599
WNC_1000	1170.3	1045.9	124.4	0.786	0.601	3.88	0.573

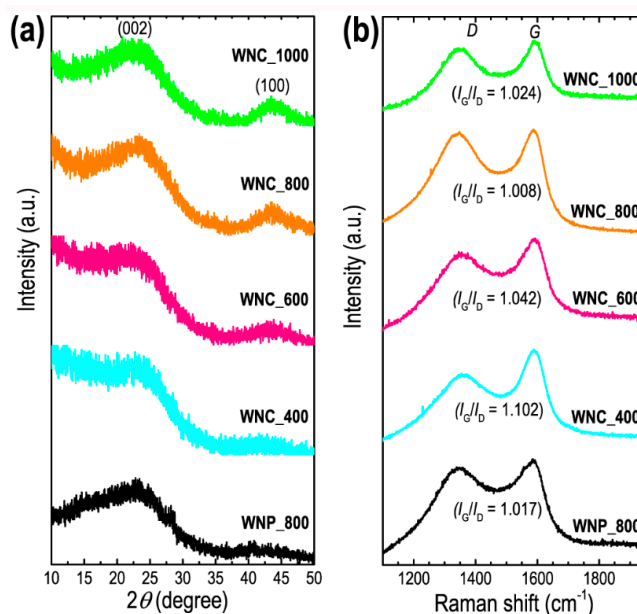
SSA (specific surface area),  $S_{\text{micro}}$  (micropore surface area),  $S_{\text{meso}}$  (mesopore surface area),  $V_p$  (total pore volume),  $V_{\text{micro}}$  (micropore volume obtained from the DFT method),  $D_{\text{meso}}$  (average mesopore diameter obtained from the BJH method), and  $D_{\text{micro}}$  (average micro diameter obtained from the DFT method) were obtained from the analysis of nitrogen sorption isotherms.

Figure 3a shows the FTIR spectrum of Washnut seed powder precursor materials before pre-carbonization or  $\text{ZnCl}_2$  activation. As expected, the precursor contains oxygen-containing functional groups ( $-\text{OH}$ ,  $\text{C}=\text{O}$ ,  $\text{COOH}$ , ether, phenol and lactones) [33,38,49]. Some of these functional groups sustain even after carbonization at high temperature. FTIR spectra of the carbon samples display a broad peak centered nearly at  $3435\text{ cm}^{-1}$  (Figure 3b), which can be attributed to the  $\text{O}-\text{H}$  functional groups and a weak FTIR peak approximately at  $1634\text{ cm}^{-1}$  come from the aromatic  $\text{C}=\text{C}$  stretching vibration commonly observed in the activated carbons [38,49].



**Figure 3.** (a) FTIR spectrum of Washnut seed powder (WNP) before activation, and (b) FTIR spectra of carbonized/activated samples WNP\_800, WNC\_400, WNC\_600, WNC\_800, and WNC\_1000 measured at  $25\text{ }^{\circ}\text{C}$ .

Powder X-ray diffraction (pXRD) and Raman scattering and analysis were also carried out to further evaluate the structural features of the Washnut seed-derived nanoporous carbon materials. Figure 4 shows the pXRD patterns and Raman scattering spectra of the prepared carbon samples.



**Figure 4.** (a) Powder X-ray diffraction (pXRD) patterns of WNP\_800, WNC\_400, WNC\_600, WNC\_800, and WNC\_1000 recorded at  $25\text{ }^{\circ}\text{C}$ , and (b) Raman scattering spectra of WNP\_800, WNC\_400, WNC\_600, WNC\_800, and WNC\_1000 recorded at  $25\text{ }^{\circ}\text{C}$ .

The pXRD patterns (Figure 4a) display characteristics of amorphous carbon with two broad peaks approximately at  $\sim 23$  and  $43^\circ$  equivalent to the (002) and (100) planes observed in graphitic carbon particles. Broad (002) diffraction profile at a diffraction angle of  $\sim 23^\circ$  indicates that the Washnut seed-derived nanoporous carbon materials have poorly ordered amorphous structure and also smaller graphitic clusters of the samples [50]. Raman spectra (Figure 4b) of all the samples exhibit *D* and *G* bands approximately at  $\sim 1350$  and  $\sim 1588$   $\text{cm}^{-1}$ , respectively [50]. The *D* band corresponds to the disordered structure of carbon induced by defects and impurities, while *G* band corresponds to the ordered graphitic layer structure. The presence of obvious *D* and *G* bands confirms the formation of activated carbons. The intensity ratio of *G* and *D* Raman bands ( $I_G/I_D$ ) measures the graphitization degree of the carbons. The  $I_G/I_D$  ratio is found in the range of 1.008 to 1.1042 characteristics of graphitic carbons commonly observed in activated carbon materials with a low degree of defects [50,51].

Electrochemical supercapacitance performance of the prepared activated nanoporous carbon materials was performed in a three-electrode system in aqueous electrolyte (1 M  $\text{H}_2\text{SO}_4$ ). Cyclic voltammetry (CV) profiles were measured in a wide scan rates of 5 to 500  $\text{mV s}^{-1}$  and galvanostatic charge-discharge (CD) curves were recorded at from 1 to 20  $\text{A g}^{-1}$  at 25  $^\circ\text{C}$ . Figure 5a compares the CV profiles of WNP\_800, WNC\_400, WNC\_600, WNC\_800, and WNC\_1000 at 5  $\text{mV s}^{-1}$  as typical example.

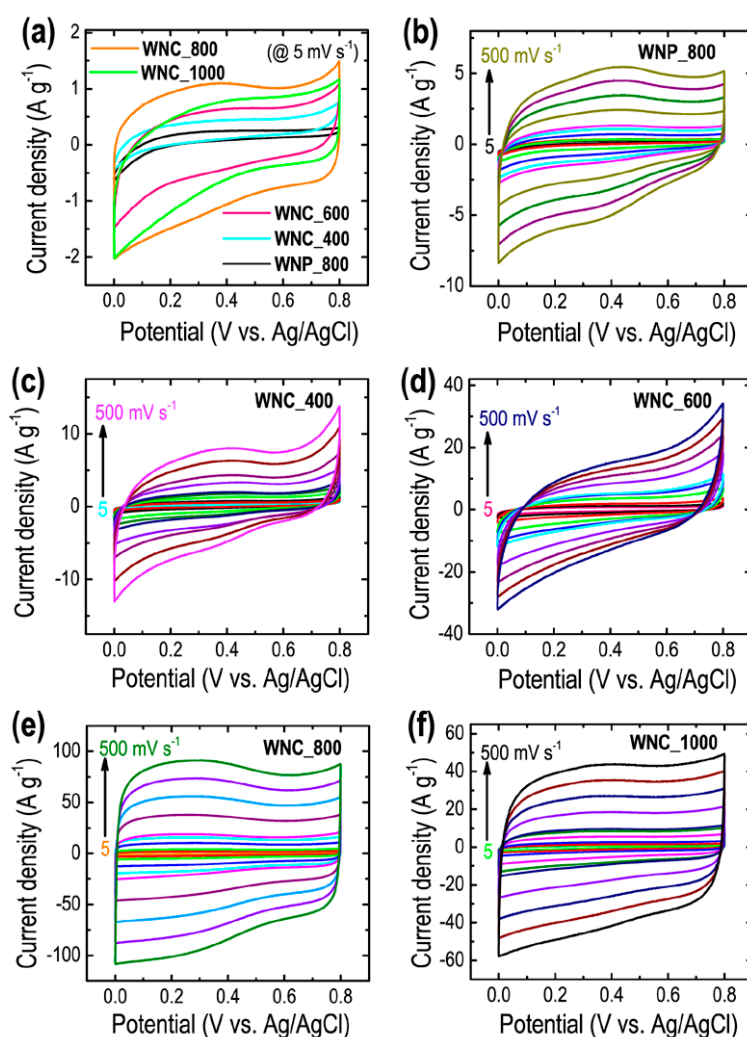


**Figure 5.** (a) Comparison of cyclic voltammetry (CV) profiles of all the prepared carbons at 5  $\text{mV s}^{-1}$ , and the CV profile vs. scan rates. (b) WNC\_800, (c) WNC\_400, (d) WNC\_600, (e) WNC\_800, and (f) WNC\_1000.

As can be seen in Figure 5a, all the CV profiles exhibit quasi-rectangular shape characteristics of the EDLC behavior [50,52]. Depending on the carbon sample, the current differs. The lowest current of the directly carbonized sample, WNP\_800, shows the poor supercapacitance performance of the materials, which can be attributed to the poor surface textural properties (surface area and porosity). The current collection under the CV profile increases with temperature up to 800 °C, i.e., from WNC\_400 to WNC\_800 sample and declines slightly in the WNC\_1000, which is directly correlated to the surface area and porosity of the carbon samples (see Table 1). Due to the highest surface area (plenty of micropores), the WNC\_800 electrode offers a large surface area for the adsorption of electrolyte ions. Furthermore, due to large porosity, and interconnected hierarchical porous structure, the electrode also offers an easy path and fast diffusion of the electrolyte ion to the electrode surface and thus showed excellent energy storage capacity. Figure 5b–f shows the CV profiles of directly carbonized sample WNP\_800, and ZnCl<sub>2</sub> activated samples WNC\_400, WNC\_600, WNC\_800, and WNC\_1000 at different scan rates from 5 to 500 mV s<sup>-1</sup>. The area under the CV profiles increases with scan rate sustaining the semi-rectangular shape of the CV curve even at the high scan rate of 500 mV s<sup>-1</sup> indicating the fast electrolyte ions diffusion [46–48,50].

The electrochemical supercapacitance performances of the WNP\_800, WNC\_400, WNC\_600, WNC\_800, and WNC\_1000 was also studied performing galvanostatic charge-discharge (CD) measurements over a wide range of current densities (1 to 20 A g<sup>-1</sup>). As seen in Figure 6a, triangular shape CD curves, which indicate the EDLC behavior of the electrode material are commonly observed in the CD profiles of WNP\_800, WNC\_400, WNC\_600, WNC\_800, and WNC\_1000 electrodes at 1 A g<sup>-1</sup> [50,53]. Here again, the CD profile of the optimal sample, WNC\_800, has the longest discharging time suggesting the maximum energy storage capacity compared to the electrodes. Using Equation (1), the C<sub>s</sub> measurements were calculated 18.3 F g<sup>-1</sup> (WNP\_800), 71.9 F g<sup>-1</sup> (WNC\_400), 155.8 F g<sup>-1</sup> (WNC\_600), 225.1 F g<sup>-1</sup> (WNC\_800), and 188.7 F g<sup>-1</sup> (WNC\_1000), which is highly interrelated with the porosity of the materials; the higher the microporosity the better the energy storage capacity (see Table 1). In Figure 6b–d, the CD profiles vs. current densities of selected samples are shown as typical examples. All the CD profiles represent characteristics of the EDLC and sustain high capacity even at 20 A g<sup>-1</sup>, a high current density. All the chemically activated nanoporous carbon materials display more than 50% capacitance retention achieving outstanding 69.6% for the optimal sample (Figure 6e), which demonstrates the high rate capability of the electrode material required in supercapacitor devices. Furthermore, cycling stability tested for the 10,000 charging-discharging cycles revealed outstanding stability with a very low capacitance loss of about 2%–3% (Figure 6f) indicating that the Washnut derived-nanoporous carbons have a huge potential and can be explored as supercapacitor electrodes [54,55].



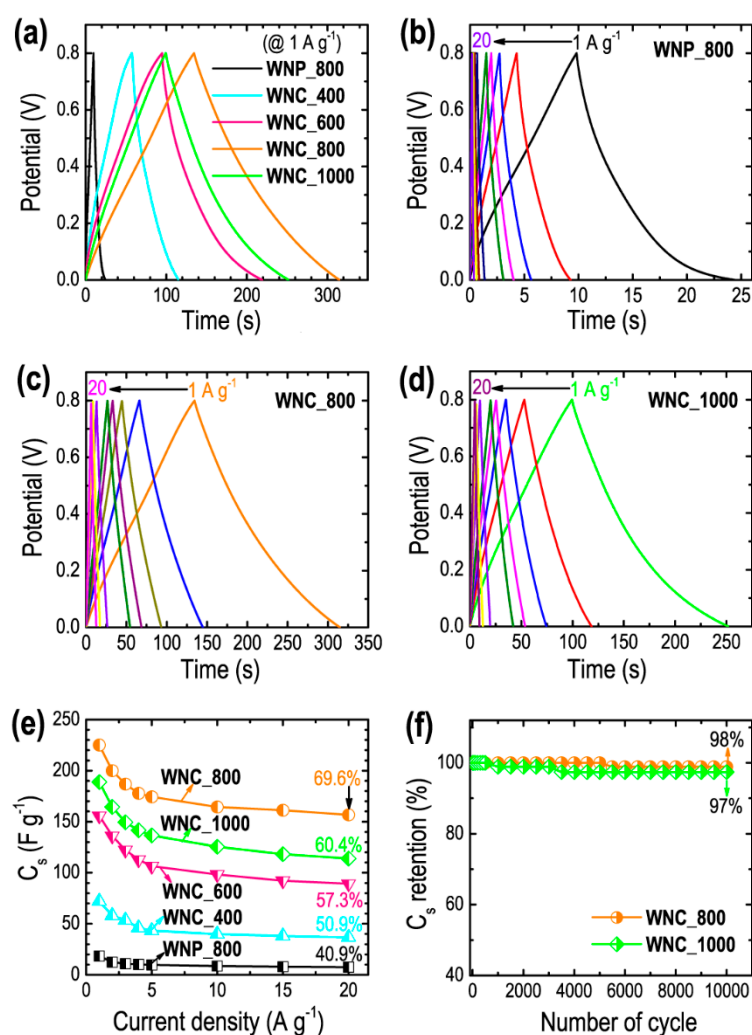


**Figure 6.** (a) Charge-discharge (CD) curves of WNP\_800, WNC\_400, WNC\_600, WNC\_800, and WNC\_1000 at a constant current density of 1 A g<sup>-1</sup>, CD profiles vs. current density for (b) WNP\_800, (c) WNC\_800, and (d) WNC\_1000 as typical examples, (e) specific capacitance (C<sub>s</sub>) vs. current density, and (g) cycling stability performances of the WNC\_800 and WNC\_1000 electrodes for 10,000 cycles as typical example.

The specific capacitance of the Washnut-derived carbon electrode is comparable with the specific capacitances of other nanoporous carbon materials prepared from different biomass (Table 2).

**Table 2.** Comparison of specific capacitance of the Washnut carbon electrode with other biomass-derived nanoporous carbon electrodes.

Biomass	Electrolyte	Current Density/Scan Rate	Specific Capacitance (F g <sup>-1</sup> )	Reference
Washnut	1 M H <sub>2</sub> SO <sub>4</sub>	1 A g <sup>-1</sup>	225.1	This work
Bio-decomposed product (Humic acids)	6 M KOH	0.05 A g <sup>-1</sup>	209	[26]
Cotton	3 M KOH	0.3 A g <sup>-1</sup>	221.7	[29]
Bamboo	1 M H <sub>2</sub> SO <sub>4</sub>	5 mV s <sup>-1</sup>	256	[31]
Corn cob	0.5 M H <sub>2</sub> SO <sub>4</sub>	0.5 A g <sup>-1</sup>	210	[39]
Lapsi seed	1 M H <sub>2</sub> SO <sub>4</sub>	1 A g <sup>-1</sup>	284	[46]
Beech ( <i>Fagus sylvatica</i> )	1 M KOH	20 mA g <sup>-1</sup>	133	[56]

The obtained specific capacitance of  $225.1 \text{ F g}^{-1}$  is not sufficient for the design of high energy density advanced supercapacitors [32,33,48,55]. Several previous examples have demonstrated that the electrochemical supercapacitive performance of the nanoporous carbon materials depends on the various important parameters such as surface area, porosity, pore size distribution, the hierarchy on the pore (micro/mesopore) architecture, and interconnectivity of the mesopores for easy electrolyte ion diffusion, conductivity, and wettability of the electrode surface [48]. Tailoring micro-porosity, nitrogen-doping, and composite preparation with pseudocapacitive metal oxide nanoparticles would offer effective strategies to enhance the supercapacitance of biomass-derived nanoporous carbons to address the social demands.

#### 4. Conclusions

In conclusion, nanoporous activated carbon materials have been prepared by  $\text{ZnCl}_2$  activation of Washnut seed powder and their electrochemical supercapacitance performances have been investigated in an aqueous electrolyte ( $1 \text{ M H}_2\text{SO}_4$ ) on a three-electrode cell. Specific surface area and pore volume were found in the ranges  $922\text{--}1309 \text{ m}^2 \text{ g}^{-1}$  and  $0.577\text{--}0.789 \text{ cm}^3 \text{ g}^{-1}$ , respectively, depending on carbonization temperatures. Because of the excellent textural properties including high surface areas, well-developed porosity, and bimodal micro- and meso-pore architecture with graphitic pore walls, the Washnut seed-derived nanoporous activated carbons display outstanding supercapacitance such that the electrode achieved a high specific capacitance of  $225.1 \text{ F g}^{-1}$  at a current density of  $1 \text{ A g}^{-1}$  and retained a high rate capability of 69.6% at  $20 \text{ A g}^{-1}$ . Furthermore, the electrode showed excellent cycling stability sustaining 98% capacity retention even after 10,000 charge-discharge cycles. Therefore, it can be concluded that as an agricultural waste, Washnut seed denotes a suitable biomass for the scalable production of high surface area and large porosity carbons essentially desired as the electrode materials for high-performance supercapacitors.

**Author Contributions:** L.K.S., R.G.S. and R.L.S. designed the experiments; R.L.S., T.S. and B.M.T. prepared the carbon materials; S.M., B.M.T. and R.L.S. characterized the materials; T.S. and R.G.S. performed the electrochemical measurements; R.L.S., R.G.S., L.K.S. and K.A. discussed the data and summarized the results; R.G.S. and R.L.S. prepared original draft; L.K.S. reviewed, edited and finalized the manuscript; K.A. and L.K.S. managed the funding acquisition. All authors have read and agreed to the published version of the manuscript.

**Funding:** This work is partially supported by supported by JSPS KAKENHI Grant Number JP 16H06518 (Coordination Asymmetry), CREST JST Grant Number JPMJCR1665, and Grants-in-Aid for Scientific Research (C) Grant Number 20K05590.

**Conflicts of Interest:** The authors declare no conflict of interest.

#### References

1. Zhao, F.; Liu, W.; Qiu, T.; Gong, W.-B.; Ma, W.; Li, Q.; Li, F.; Geng, F. All two-dimensional pseudocapacitive sheet materials for flexible asymmetric solid-state planar microsupercapacitors with high energy density. *ACS Nano* **2020**, *14*, 603–610. [[CrossRef](#)] [[PubMed](#)]
2. Lin, Y.; Chem, Z.; Yu, C.; Zhong, W. Facile synthesis of high nitrogen-doped content, mesopore-dominated biomass-derived hierarchical porous graphitic carbon for high performance supercapacitors. *Electrochim. Acta* **2020**, *334*, 135615. [[CrossRef](#)]
3. Ellessawy, N.A.; El Nady, J.; Wazeer, W.; Kashyout, A.B. Development of high-performance supercapacitor based on a novel controllable green synthesis for 3D nitrogen doped graphene. *Sci. Rep.* **2019**, *9*, 1129. [[CrossRef](#)] [[PubMed](#)]
4. Shao, Y.; El-Kady, M.F.; Sun, J.; Li, Y.; Zhang, Q.; Zhu, M.; Wang, H.; Dunn, B.; Kaner, R.B. Design and mechanisms of asymmetric supercapacitors. *Chem. Rev.* **2018**, *118*, 9233–9280. [[CrossRef](#)] [[PubMed](#)]
5. An, T.; Cheng, W. Recent progress in stretchable supercapacitors. *J. Mater. Chem. A* **2018**, *6*, 15478–15494. [[CrossRef](#)]
6. Han, Y.; Lai, Z.; Wang, Z.; Yu, M.; Tong, Y.; Lu, X. Designing carbon based supercapacitors with high energy density: A summary of recent progress. *Chem. Eur. J.* **2018**, *24*, 7312–7329. [[CrossRef](#)]

7. Wang, F.; Wu, X.; Yuan, X.; Liu, Z.; Zhang, Y.; Fua, L.; Zhu, Y.; Zhou, Q.; Wu, Y.; Huang, W. Latest advances in supercapacitors: From new electrode materials to novel device designs. *Chem. Soc. Rev.* **2017**, *46*, 6816–6854. [[CrossRef](#)]
8. Vellacheri, R.; Al-Haddad, A.; Zhao, H.; Wang, W.; Wang, C.; Lei, Y. High performance supercapacitor for efficient energy storage under extreme environmental temperatures. *Nano Energy* **2014**, *8*, 231–237. [[CrossRef](#)]
9. Wang, Y.; Xia, Y. Recent progress in supercapacitors: From materials design to system construction. *Adv. Mater.* **2013**, *25*, 5336–5342. [[CrossRef](#)]
10. Simon, P.; Gogotsi, Y. Materials for electrochemical capacitors. *Nat. Mater.* **2008**, *7*, 845–854. [[CrossRef](#)]
11. Ji, H.; Zhao, X.; Qiao, Z.; Jung, J.; Zhu, Y.; Lu, Y.; Zhang, L.L.; MacDonald, A.H.; Ruoff, R.S. Capacitance of carbon-based electrical double-layer capacitors. *Nat. Commun.* **2014**, *5*, 3317. [[CrossRef](#)] [[PubMed](#)]
12. Miller, J.R.; Simon, P. Electrochemical capacitors for energy management. *Science* **2008**, *321*, 651–652. [[CrossRef](#)] [[PubMed](#)]
13. Frenzel, B.; Kurzweil, P.; Rönnebeck, H. Electromobility concept for racing cars based on lithium-ion batteries and supercapacitors. *J. Power Sources* **2011**, *196*, 5364–5376. [[CrossRef](#)]
14. Kouchachvili, L.; Yaïci, W.; Entchev, E. Hybrid battery/supercapacitor energy storage system for the electric vehicles. *J. Power Sources* **2018**, *374*, 237–248. [[CrossRef](#)]
15. Hannan, M.A.; Lipu, M.S.H.; Hussain, A.; Mohamed, A. A review of lithium-ion battery state of charge estimation and management system in electric vehicle applications: Challenges and recommendations. *Renew. Sustain. Energy Rev.* **2017**, *78*, 834–854. [[CrossRef](#)]
16. Stoller, M.D.; Ruoff, R.S. Best practice methods for determining an electrode material's performance for ultracapacitors. *Energy Environ. Sci.* **2010**, *3*, 1294–1301. [[CrossRef](#)]
17. Pal, B.; Yang, S.; Ramesh, S.; Thangadurai, V.; Jose, R. Electrolyte selection for supercapacitive devices: A critical review. *Nanoscale Adv.* **2019**, *1*, 3807–3835. [[CrossRef](#)]
18. Chen, K.; Xue, D. Searching for electrode materials with high electrochemical reactivity. *J. Mater.* **2015**, *1*, 170–187. [[CrossRef](#)]
19. Xu, X.; Yang, T.; Zhang, Q.; Xia, W.; Ding, Z.; Eid, K.; Abdullah, A.M.; Hossain, M.S.A.; Zhang, S.; Tang, J.; et al. Ultrahigh capacitive deionization performance by 3D interconnected MOF-derived nitrogen-doped carbon tubes. *Chem. Eng. J.* **2020**, *390*, 124493. [[CrossRef](#)]
20. Szubzda, B.; Szmaja, A.; Halama, A. Influence of structure and wettability of supercapacitor electrodes carbon materials on their electrochemical properties in water and organic solutions. *Electrochim. Acta* **2012**, *86*, 255–259. [[CrossRef](#)]
21. Largeot, C.; Portet, C.; Chmiola, J.; Taberna, P.-L.; Gogotsi, Y.; Simon, P. Relation between the ion size and pore size for an electric double-layer capacitor. *J. Am. Chem. Soc.* **2008**, *130*, 2730–2731. [[CrossRef](#)] [[PubMed](#)]
22. Wang, G.; Zhang, L.; Zhang, J. A review of electrode materials for electrochemical supercapacitors. *Chem. Soc. Rev.* **2012**, *41*, 797–828. [[CrossRef](#)] [[PubMed](#)]
23. Dutta, S.; Bhaumik, A.; Wu, K.C.-W. Hierarchically porous carbon derived from polymers and biomass: Effect of interconnected pores on energy applications. *Energy Environ. Sci.* **2014**, *7*, 3574–3592. [[CrossRef](#)]
24. Magana, J.R.; Kolen'ko, Y.V.; Deepak, F.L.; Solans, C.; Shrestha, R.G.; Hill, J.P.; Ariga, K.; Shrestha, L.K.; Rodriguez-Abreu, C. From chromonic self-assembly to hollow carbon nanofibers: Efficient materials in supercapacitor and vapor-sensing applications. *ACS Appl. Mater. Interfaces* **2016**, *8*, 31231–31238. [[CrossRef](#)]
25. Shi, Y.; Zhang, L.; Schon, T.B.; Li, H.; Fan, C.; Li, X.; Wang, H.; Wu, X.; Xie, H.; Sun, H.; et al. Porous carbon with Willow-leaf-shaped pores for high-performance supercapacitors. *ACS Appl. Mater. Interfaces* **2017**, *9*, 42699–42707. [[CrossRef](#)] [[PubMed](#)]
26. Zhu, Y.; Chen, M.; Zhang, Y.; Zhao, W.; Wang, C. A biomass-derived nitrogen-doped porous carbon for high-energy supercapacitor. *Carbon* **2018**, *140*, 404–412. [[CrossRef](#)]
27. Tang, Q.; Bairei, P.; Shrestha, R.G.; Hill, J.P.; Ariga, K.; Zeng, H.; Ji, Q.; Shrestha, L.K. Quasi 2D mesoporous carbon microbelts derived from fullerene crystals as an electrode material for electrochemical supercapacitors. *ACS Appl. Mater. Interfaces* **2017**, *9*, 44458–44465. [[CrossRef](#)] [[PubMed](#)]
28. Bairei, P.; Shrestha, R.G.; Hill, J.P.; Nishimura, T.; Ariga, K.; Shrestha, L.K. Mesoporous graphitic carbon microtubes derived from fullerene C<sub>70</sub> tubes as a high performance electrode material for advanced supercapacitors. *J. Mater. Chem. A* **2016**, *4*, 13899–13906. [[CrossRef](#)]
29. Liu, Y.; Shi, Z.; Gao, Y.; An, W.; Cao, Z.; Liu, J. Biomass-swelling assisted synthesis of hierarchical porous carbon fibers for supercapacitor electrodes. *ACS Appl. Mater. Interfaces* **2016**, *8*, 28283–28290. [[CrossRef](#)]

30. Salunkhe, R.R.; Kaneti, Y.V.; Kim, J.; Kim, J.H.; Yamauchi, Y. Nanoarchitectures for metal–organic framework-derived nanoporous carbons toward supercapacitor applications. *Acc. Chem. Res.* **2016**, *49*, 2796–2806. [[CrossRef](#)]
31. Shrestha, L.K.; Adhikari, L.; Shrestha, R.G.; Adhikari, M.P.; Adhikari, R.; Hill, J.P.; Pradhananga, R.R.; Ariga, K. Nanoporous carbon materials with enhanced supercapacitance performance and non-aromatic chemical sensing with C<sub>1</sub>/C<sub>2</sub> alcohol discrimination. *Sci. Technol. Adv. Mater.* **2016**, *17*, 483–492. [[CrossRef](#)] [[PubMed](#)]
32. Yang, S.; Wang, S.; Liu, X.; Li, L. Biomass derived interconnected hierarchical micro-meso-macroporous carbon with ultrahigh capacitance for supercapacitors. *Carbon* **2019**, *147*, 540–549. [[CrossRef](#)]
33. Cao, Y.; Xie, L.; Sun, G.; Su, F.; Kong, Q.-Q.; Li, F.; Ma, W.; Shi, J.; Jiang, D.; Lu, C.; et al. Hollow carbon microtubes from kapok fiber: Structural evolution and energy storage performance. *Sustain. Energy Fuels* **2018**, *2*, 455–465. [[CrossRef](#)]
34. Fan, W.; Zhang, H.; Wang, H.; Zhao, X.; Sun, S.; Shi, J.; Huang, M.; Liu, W.; Zheng, Y.; Li, P. Dual-doped hierarchical porous carbon derived from biomass for advanced supercapacitors and lithium ion batteries. *RSC Adv.* **2019**, *9*, 32382–32394. [[CrossRef](#)]
35. Kaipannan, S.; Marappan, S. Fabrication of 9.6 V high-performance asymmetric supercapacitors stack based on nickel hexacyanoferrate-derived Ni(OH)<sub>2</sub> nanosheets and bio-derived activated carbon. *Sci. Rep.* **2019**, *9*, 1104. [[CrossRef](#)] [[PubMed](#)]
36. Liu, S.; Pan, M.; Feng, Z.; Qin, Y.; Wang, Y.; Tan, L.; Sun, T. Ultra-high adsorption of tetracycline antibiotics on garlic skin-derived porous biomass carbon with high surface area. *New J. Chem.* **2020**, *44*, 1097–1106. [[CrossRef](#)]
37. Ghosh, S.; Santhosh, R.; Jeniffer, S.; Raghavan, V.; Jacob, G.; Nanaji, K.; Kollu, P.; Jeong, S.K.; Grace, A.N. Natural biomass derived hard carbon and activated carbons as electrochemical supercapacitor electrodes. *Sci. Rep.* **2019**, *9*, 16315. [[CrossRef](#)]
38. Shrestha, L.K.; Thapa, M.; Shrestha, R.G.; Maji, S.; Pradhananga, R.R.; Ariga, K. Rice husk-derived high surface area nanoporous carbon materials with excellent iodine and methylene blue adsorption properties. *C J. Carbon Res.* **2019**, *5*, 10. [[CrossRef](#)]
39. Genovese, M.; Jiang, J.; Lian, K.; Holmb, N. High capacitive performance of exfoliated biochar nanosheets from biomass waste corn cob. *J. Mater. Chem. A* **2015**, *3*, 2903–2913. [[CrossRef](#)]
40. Liu, Y.; Xiao, Z.; Liu, Y.; Fan, L.-Z. Biowaste-derived 3D honeycomb-like porous carbon with binary-heteroatom doping for high-performance flexible solid-state supercapacitors. *J. Mater. Chem. A* **2018**, *6*, 160–166. [[CrossRef](#)]
41. Niksiar, A.; Nasernejad, B. Activated carbon preparation from pistachio shell pyrolysis and gasification in a spouted bed reactor. *Biomass Bioenergy* **2017**, *106*, 43–50. [[CrossRef](#)]
42. Gao, F.; Geng, C.; Xiao, N.; Qu, J.; Qiu, J. Hierarchical porous carbon sheets derived from biomass containing an activation agent and in-built template for lithium ion batteries. *Carbon* **2018**, *139*, 1085–1092. [[CrossRef](#)]
43. Li, J.; Wu, Q. Water bamboo-derived porous carbons as electrode materials for supercapacitors. *New J. Chem.* **2015**, *39*, 3859–3864. [[CrossRef](#)]
44. Wei, X.; Li, Y.; Gao, S. Biomass-derived interconnected carbon nanoring electrochemical capacitors with high performance in both strongly acidic and alkaline electrolytes. *J. Mater. Chem. A* **2017**, *5*, 181–188. [[CrossRef](#)]
45. Yuan, G.; Huang, W.; Guan, K.; Li, H.; Xie, Y.; Liang, Y.; Liu, Y.; Zheng, M. A universal KOH-free strategy towards nitrogen doped carbon nanosheets for high-rate and high energy storage devices. *J. Mater. Chem. A* **2019**, *7*, 26469–26478. [[CrossRef](#)]
46. Shrestha, L.K.; Shrestha, R.G.; Maji, S.; Pokahrel, B.P.; Rajbhandari, R.; Shrestha, R.L.; Pradhananga, R.R.; Hill, J.P.; Ariga, K. High surface area nanoporous graphitic carbon materials derived from Lapsi seed with enhanced supercapacitance. *Nanomaterials* **2020**, *10*, 728. [[CrossRef](#)] [[PubMed](#)]
47. Tang, J.; Wang, J.; Shrestha, L.K.; Hossain, S.A.; Allothman, Z.A.; Yamauchi, Y.; Ariga, K. Activated Porous Carbon Spheres with Customized Mesopores through Assembly of Diblock Copolymers for Electrochemical Capacitor. *ACS Appl. Mater. Interfaces* **2017**, *9*, 18986–18993. [[CrossRef](#)] [[PubMed](#)]
48. Shrestha, R.G.; Maji, S.; Shrestha, L.K.; Ariga, K. Nanoarchitectonics of nanoporous carbon materials in supercapacitors applications. *Nanomaterials* **2020**, *10*, 639. [[CrossRef](#)] [[PubMed](#)]

49. Hesas, R.H.; Arami-Niya, A.; Daud, W.M.A.W.; Sahu, J.N. Preparation and characterization of activated carbon from apple waste by microwave-assisted phosphoric acid activation: Application in methylene blue adsorption. *BioResources* **2013**, *8*, 2950–2966.
50. Zhu, Y.; Murali, S.; Stoller, M.D.; Ganesh, K.J.; Cai, W.; Ferreira, P.J.; Pirkle, A.; Wallace, R.M.; Cychosz, K.A.; Thommes, M.; et al. Carbon-based supercapacitors produced by activation of graphene. *Science* **2011**, *332*, 1537–1541. [[CrossRef](#)]
51. Hirst, E.A.; Taylor, A.; Mokaya, R. A simple flash carbonization route for conversion of biomass to porous carbons with high CO<sub>2</sub> storage capacity. *J. Mater. Chem. A* **2018**, *6*, 12393–12403. [[CrossRef](#)]
52. Lee, J.-S.M.; Briggs, M.E.; Hu, C.-C.; Cooper, A.I. Controlling electric double-layer capacitance and pseudocapacitance in heteroatom-doped carbons derived from hypercrosslinked microporous polymers. *Nano Energy* **2018**, *46*, 277–289. [[CrossRef](#)]
53. Wang, Y.; Song, Y.; Xia, Y. Electrochemical capacitors: Mechanism, materials, systems, characterization and applications. *Chem. Soc. Rev.* **2016**, *45*, 5925–5950. [[CrossRef](#)] [[PubMed](#)]
54. Zhou, S.; Zhou, L.; Zhang, Y.; Sun, J.; Wen, J.; Yuan, Y. Upgrading earth-abundant biomass into three dimensional carbon materials for energy and environmental applications. *J. Mater. Chem. A* **2019**, *7*, 4217–4229. [[CrossRef](#)]
55. Bi, Z.; Kong, Q.; Cao, Y.; Sun, G.; Su, F.; Wei, X.; Li, X.; Ahmad, A.; Xie, L.; Chen, C.-M. Biomass-derived porous carbon materials with different dimensions for supercapacitor electrodes: A review. *J. Mater. Chem. A* **2019**, *7*, 16028–16045. [[CrossRef](#)]
56. Gutiérrez-Pardo, A.; Ramírez-Rico, J.; Cabezas-Rodríguez, R.; Martínez-Fernández, J. Effect of catalytic graphitization on the electrochemical behavior of wood derived carbons for use in supercapacitors. *J. Power Sources* **2015**, *278*, 18–26. [[CrossRef](#)]



© 2020 by the authors. Licensee MDPI, Basel, Switzerland. This article is an open access article distributed under the terms and conditions of the Creative Commons Attribution (CC BY) license (<http://creativecommons.org/licenses/by/4.0/>).